Journal of Solid State Chemistry 184 (2011) 141–148

Contents lists available at ScienceDirect

Journal of Solid State Chemistry

journal homepage: www.elsevier.com/locate/jssc

One-dimensional $GdVO_4$:Ln^{3+} (Ln=Eu, Dy, Sm) nanofibers: Electrospinning preparation and luminescence properties

Xue Li [a,b], Min Yu [a,b], Zhiyao Hou [a], Guogang Li [a], Ping'an Ma [a,*], Wenxin Wang [a], Ziyong Cheng [a], Jun Lin [a,*]

[a] State Key Laboratory of Rare Earth Resource Utilization, Changchun Institute of Applied Chemistry, Chinese Academy of Sciences, Changchun 130022, PR China
[b] Department of Chemistry, Northeast Normal University, Changchun 130024, PR China

ARTICLE INFO

Article history:
Received 16 May 2010
Received in revised form
27 October 2010
Accepted 11 November 2010
Available online 18 November 2010

Keywords:
Electrospinning
Vanadate
Lanthanide
Luminescence
Nanofibers

ABSTRACT

One-dimensional $GdVO_4$:Ln^{3+} (Ln=Eu, Dy, Sm) nanofibers have been prepared by a combination method of sol–gel process and electrospinning technology. X-ray diffraction (XRD), Fourier transform infrared spectroscopy (FT-IR), thermogravimetric and differential thermal analysis (TG-DTA), scanning electron microscopy (SEM), transmission electron microscopy (TEM), photoluminescence (PL), quantum efficiency (QE), and cathodoluminescence (CL) spectra as well as kinetic decays were used to characterize the samples. The XRD, FT-IR, and TG-DTA results show that $GdVO_4$:Ln^{3+} nanofibers samples crystallize at 700 °C. SEM images indicate that the as prepared precursor fibers are smooth. After being calcined at 700 °C for 4 h, the fibers still maintain their fiberlike morphology with rough surface. TEM image further manifests that the $GdVO_4$:Ln^{3+} nanofibers consist of nanoparticles. Under ultraviolet excitation and low-voltage electron beam excitation, $GdVO_4$:Ln^{3+} phosphors showed their strong characteristic emission due to an efficient energy transfer from vanadate groups to dopants. The optimum doping concentration of Ln^{3+} in the $GdVO_4$ nanofibers also has been investigated.

1. Introduction

As is well known, shape and dimensionality are regarded as particularly important factors that influence the properties of materials. Thus, dramatic efforts have been dedicated to fabricate a range of high-quality inorganic nanomaterials with different morphology. In recent years, much attentions has been paid to preparation of one-dimensional (1D) nanaomaterials including nanowires (NWs), nanorods, nanotubes (NTs), and nanobelts, which exhibit novel physical and chemical properties due to their unique and fascinating characteristics for huge ratio of diameter to length, superior mechanical toughness, and so on [1–6]. One-dimensional (1D) nanomaterials also play an important role in both fundamental research and technological applications [7–9]. It has been reported that the Eu^{3+} ions have shown higher quantum efficiency values in 1D $LaPO_4$ nanowires (via the hydrothermal process) than in 0D $LaPO_4$ nanoparticles and the corresponding bulk materials [10–13]. But it is not easy to control the 1D nanostructures by the hydrothermal process. So it is important to develop some facile synthesis methods to directly prepare luminescent materials in nano-/microscale with defined morphologies. Now, many methods have been used to prepare one-dimensional (1D) nanomaterials with different composition, including chemical or physical vapor deposition [14–17], solution [18], arc discharge [19,20], laser ablation [14,21], vapor-phase transport process [22–24], and a template-based method [25–27]. Among the various methods, electrospinning is a more simple, effective, and cost-effective approach for generating long fibers with diameters ranging from tens of nanometers up to micrometers. Electrospinning technology has been used to prepare one-dimensional (1D) nanomaterials since 1930s [28]. Organic, inorganic, and hybrid (organic–inorganic) compounds [29–32] all can be electrospun to form uniform fibers. The sol–gel technique has been proved as an efficient way to produce nanoparticles [33], which can be employed to prepare precursor solution. A combination method of sol–gel process and electrospinning technique is a good approach to obtain excellent 1D and Q-1D nano-/microstructures, which can be applied in sensors, electronic and optical device, biomedical fields, and catalyst supports [34–37]. Accordingly, the preparation of 1D vanadate nanofibers by the novel and facile sol–gel/electrospinning process and investigation on their luminescence properties will be of great interest and importance.

Rare earth oxides have been extensively used in high performance luminescent devices due to higher chemical stability than other phosphors such as sulfide phosphors [38,39]. Many investigations [40,41] have been drawn to rare earth vanadates because they are excellent hosts for luminescence materials. Furthermore, gadolinium vanadate is also a promising material for lanthanide ion doped oxide phosphors and near-infrared lasers. In the fields of luminescent material, phosphors based on gadolinium compounds also play an important role because the Gd^{3+} ion ($4f^7$,^8S) has its lowest excited level at relatively high energy, which is due to the

* Corresponding authors. Fax: +86 431 85698041.
E-mail address: jlin@ciac.jl.cn (J. Lin).

0022-4596/$ - see front matter © 2010 Elsevier Inc. All rights reserved.
doi:10.1016/j.jssc.2010.11.019

stability of the half-filled shell ground state [38,42]. Gadolinium vanadate crystal as the host of lanthanide ion was first introduced by Zaguniennyi et al. in 1992 [43]. They found that gadolinium vanadate crystal had more advantages than yttrium vanadate crystal such as higher thermal conductivity, lager emission cross-section, and larger absorption cross-section, which was considered to be suitable for laser materials. $GdVO_4$:Eu^{3+} is a highly efficient red light-emitting material due to a strong absorption of ultraviolet light by $GdVO_4$ and an efficient energy transfer from VO_4^{3-} groups to Eu^{3+}, which can be applied in many fields, such as cathode ray tubes, lamps, X-ray detectors [44–47]. If $GdVO_4$:Eu^{3+} was fabricated in the form of a 1D nanostructure, it would be expected to be highly functional material [48,49]. Besides Eu^{3+} ion, Dy^{3+} and Sm^{3+} ions can also act as useful activators. Frequently, Dy^{3+} as activator ions mainly shows emission due to transitions of $^4F_{9/2}$–$^6H_{13/2}$ in the blue region and $^4F_{9/2}$–$^6H_{15/2}$ in the yellow region, Sm^{3+} as activator ions mainly shows emission due to transitions of ($^4G_{5/2}$–$^6H_{5/2}$) in the green region, ($^4G_{5/2}$–$^6H_{7/2}$) in the orange region, and ($^4G_{5/2}$–$^6H_{9/2}$) in the red region. As far as we know, no study has been reported on synthesis of 1D $GdVO_4$:Ln^{3+} (Ln=Eu, Dy, Sm) phosphor materials via the electrospinning process. Therefore, in this paper, we prepared 1D $GdVO_4$:Ln^{3+} (Ln=Eu, Dy, Sm) nanofibers by a combination method of sol–gel process and simple electrospinning technology, and investigated the morphology, structure, photoluminescence, and cathodoluminescence properties of the resulting samples in detail.

2. Experimental section

2.1. Chemicals and materials

Gd_2O_3, Eu_2O_3, Dy_2O_3, and Sm_2O_3 (99.99%) were purchased from Science and Technology Parent Company of Changchun Institute of Applied Chemistry. NH_4VO_3 (99%, analytical reagent, AR) was purchased from Tianjing Damao Chemicals Company. Nitric acid HNO_3 (AR), citric acid monohydrate $C_6H_8O_7 \cdot H_2O$ ($\geq$99.5%, AR), and ethanol were all purchased from Beijing Fine Chemical Company. Polyvinylpyrrolidone (PVP, Mw=1,300,000) was purchased from Aldrich. All the initial chemicals in this paper were used without further purification.

2.2. Preparation

$GdVO_4$:Ln^{3+} (Ln=Eu, Dy, Sm) nanofibers were prepared by an electrospinning process followed by annealing at high temperature. The doping concentrations of Ln^{3+} are 1–10 mol% of Gd^{3+} in $GdVO_4$. First, the precursor solution for electrospinning was prepared by the sol–gel technique. The stoichiometric amounts of Gd_2O_3, Eu_2O_3, Dy_2O_3, Sm_2O_3, and NH_4VO_3 were dissolved in dilute nitric acid under heating, and then mixed with water–ethanol (v/v=3:7) solution containing a suitable amount of citric acid (the molar ratio of metal ions to citric acid is 1:2) as a chelating agent for metal ions. Then a certain amount of PVP was added into above solution to form a viscous solution for electrospinning. The weight percentage of PVP was 8% in the water–ethanol solution. After that, the precursor solution was stirred for 4 h to form a homogeneous hybrid solution for electrospinning. Then above precursor solution was loaded into a 5 mL syringe with a flat tip needle. The anode from a high-voltage power was connected with the syringe needle flat tip. The cathode was linked to the grounded collector, and the distance between needle and collector was fixed at 17 cm. The high-voltage power supply was maintained at 13 kV, and the flow rate of spinning solution was controlled at 0.5 mL/h by a syringe pump (TJ-3A/W0109-1B, Boading Longer Precision Pump Co., Ltd., China). In this way, the precursor fibers were prepared. Finally, the as-prepared electrospun fibers were calcined to the desired temperature 700 °C for 4 h with a heating rate of 2 °C/min to remove organic species.

2.3. Characterization

The X-ray powder diffraction (XRD) measurements were carried out on a Rigaku-Dmax 2500 diffractometer using Cu$K\alpha$ radiation (λ=0.15405 nm). FT-IR spectra were measured with a Perkin-Elmer 580B infrared spectrophotometer with the KBr pellet technique. Thermogravimetric and differential thermal analysis (TG-DTA) data were recorded with a thermal analysis instrument (SDT 2960, TA Instruments, New Castle, DE) with the heating rate of 10 °C min^{-1} in an air flow of 100 mL min^{-1}. The morphology and structure of the samples were inspected using a field emission scanning electron microscope (FESEM, XL30, Philips). Transmission electron microscopy (TEM) and high-resolution transmission electron microscopy (HRTEM) micrographs were obtained from a FEI Tecnai G2 S-Twin transmission electron microscope with a field emission gun operating at 200 kV. The photoluminescence (PL) measurements were performed on a Hitachi F-7000 spectrophotometer equipped with a 150 W xenon lamp as the excitation source. The cathodoluminescent (CL) measurements were carried out in an ultrahigh-vacuum chamber ($<10^{-8}$ Torr), where the samples were excited by an electron beam at a voltage range of 3–5 kV with different filament currents, and the emission spectra were recorded using an F-7000 spectrophotometer. The luminescence decay curves were obtained from a Lecroy Wave Runner 6100 digital oscilloscope (1 GHz) using a tunable laser (pulse width=4 ns, gate=50 ns) as excitation source (Continuum Suncite OPO). The absolute quantum efficiencies of the phosphor samples were measured on the C9920-02 quantum yield measurement system (Hamamatsu Photonics K.K., Japan). All the measurements were performed at room temperature (RT).

3. Results and discussion

3.1. Formation and morphology

3.1.1. XRD

XRD patterns of the as prepared precursor fibers for $GdVO_4$:Ln^{3+} (Ln=5 mol% Eu, 2 mol% Dy, 2 mol% Sm) and those calcined at 700 °C for 4 h, as well as the standard card of $GdVO_4$ (JCPDS no. 17-0260) are shown in Fig. 1, respectively. In Fig. 1a for the as prepared precursor

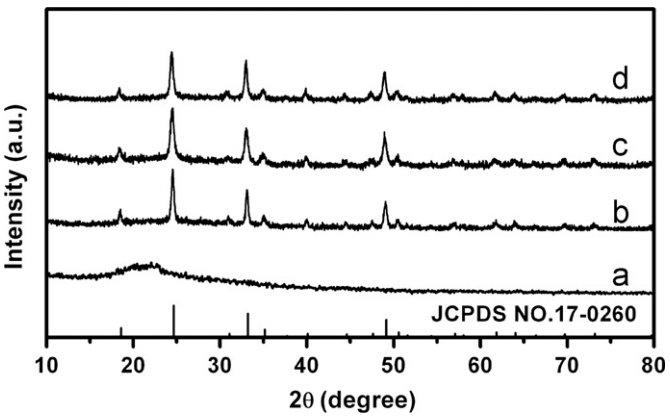

Fig. 1. XRD patterns of the $GdVO_4$:Ln^{3+} nanofibers: (a) as prepared precursor fibers, (b) the $GdVO_4$:5 mol% Eu^{3+} precursor annealed at 700 °C, (c) the $GdVO_4$:2 mol% Dy^{3+} precursor fibers annealed at 700 °C, (d) the $GdVO_4$:2 mol% Sm^{3+} precursor fibers annealed at 700 °C, as well as the standard card (JCPDS 17-0260) of $GdVO_4$ for comparison.

sample, no diffraction peak is observed except for a broad band at $2\theta = 22^\circ$, which is ascribed to the semicrystalline PVP. When $GdVO_4$:Ln^{3+} precursor samples were annealed at 700 °C (in Fig. 2b–d), well-defined diffraction peaks appeared, and all the diffraction peaks can be well-assigned to tetragonal $GdVO_4$ (JCPDS no. 17-0260). This manifests that the precursor samples have crystallized into $GdVO_4$ at this temperature. No peak from second phase is observed, indicating that the Ln^{3+} ions have been effectively built into $GdVO_4$ host lattice by substitution for the Gd^{3+} ions.

3.1.2. FT-IR

Fig. 2 displays the FT-IR spectra of the as prepared precursor fibers for $GdVO_4$:5 mol% Eu^{3+} and those heat-treated at 700 °C. In Fig. 2a, a broad band at 3426 cm^{-1} is assigned to the symmetric stretching of –OH group. Some other vibration bands of the $-CH_2$ group (2957, 1465, and 1424 cm^{-1}), $-C=O$ group (1656 cm^{-1}), carbonates COO^- group (1384 cm^{-1}), and tertiary amine group (1291 cm^{-1}) can also be detected, which come from precursor fibers (ethanol, citric acid, and PVP) [50–52]. After the precursor fibers were calcined at 700 °C for 4 h (Fig. 2b), the absorption peaks of vibration bands from precursor fibers disappear, two new absorption bands are presented. The stronger peak centered at 806 cm^{-1} and the weak peak centered 452 cm^{-1} are attributed to the absorption of V–O (from the VO_4^{3-} group) [53] and Gd–O bonds [54], respectively. This indicates that crystalline-phase $GdVO_4$ has formed after annealing at 700 °C, agreeing well with the results of XRD.

3.1.3. TG-DTA

TG-DTA curves of the as prepared precursor fibers for $GdVO_4$:5 mol% Eu^{3+} heat-treated in air with a heating rate of 10 °C/min are shown in Fig. 3. The TG curve displays three stages of weight loss. The weight loss (25%) of first stage (40–260 °C) comes from evaporation of water and alcohol. The second stage (260 – 368 °C) weight loss accompanied by an exothermic peak at 312 °C in the DTA curve is 54%, which can be attributed to the decomposition of organic group (PVP, citric acid, and the citrates) [55–56]. An exothermic peak at 400 °C in the DTA curve is correlated with the third stage weight loss (13%) from 368 to 510 °C, which is caused by the further combustion of residual organic compounds. When the temperature reached above 510 °C, there was no change in weight loss, indicating the formation of stable inorganic phase.

3.1.4. SEM and TEM

The morphology and structure of samples were investigated by the SEM and TEM observations. The SEM images of as prepared precursor fibers for $GdVO_4$:5 mol% Eu^{3+} and those heated at 700 °C are shown in Fig. 4. From the low-magnification SEM image of the precursor fibers (Fig. 4a) and resulting nanofibers (Fig. 4c), it can be seen that the samples consist of uniform fibers with lengths of several tens to hundreds micrometers. High-magnification SEM images show that the surface of the as prepared precursor fibers (Fig. 4b) is smooth with diameters ranging from 230 to 460 nm. After being calcined at 700 °C for 4 h (Fig. 4d), the fiber surfaces become rough and the fiber diameters decrease greatly due to the decomposition of the organic species and the formation of inorganic phase, and the diameters range from 100 to 160 nm. In fact, the morphology and diameter of the electrospun samples are dependent on several process parameters, including the intrinsic properties of the solution and the operational conditions. In order to obtain fibers with perfect uniform morphology, the key is searching for a balance point of various electrospinning parameters. The balance point might be related to the volume ratio of water to alcohol, the weight percentage of PVP, the spinning rate, the strength of the electric field, and the distance between the spinneret and the collector. The final samples (doped with various contents of Ln^{3+}) were also investigated by EDS analyses. The data indicate that the weight percentage of Ln^{3+} ions (Ln = Eu, Dy, Sm) by substituting Gd^{3+} into $GdVO_4$ lattice are 4.66%, 2.28%, and 2.32%, respectively. For the sake of clarity and simpleness in expressions, we still use the nominal compositions in the main text of the paper.

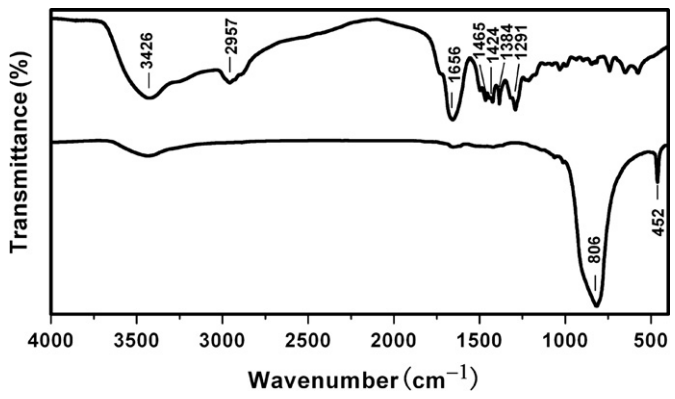

Fig. 2. FT-IR spectra of the $GdVO_4$:5 mol% Eu^{3+} nanofibers: (a) the as-prepared precursor fibers and (b) the precursor fibers annealed at 700 °C.

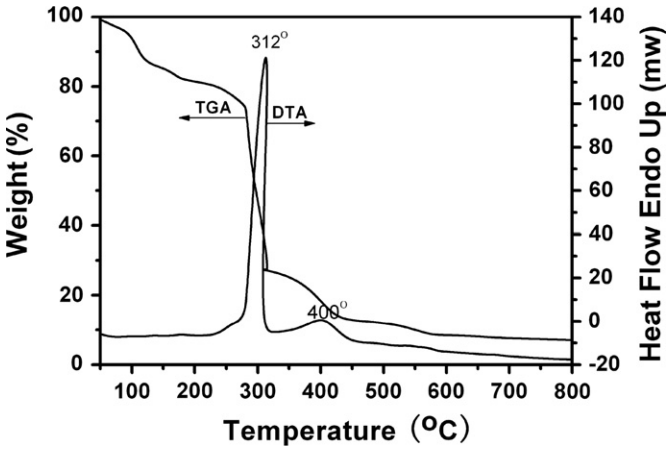

Fig. 3. TG-DTA curves of the as prepared precursor fibers of $GdVO_4$:5 mol% Eu^{3+}.

Fig. 5 shows the typical TEM and high resolution TEM (HRTEM) images of $GdVO_4$:5 mol% Eu^{3+} nanofibers annealed at 700 °C. From Fig. 5a, it can be observed that the nanofibers are composed of fine and closely linked nanoparticles (the crystallite size is about 28 nm). HRTEM image (Fig. 5b) of $GdVO_4$:5 mol% Eu^{3+} nanofibers shows well-resolved lattice fringes. The distance between the adjacent lattice fringes is 0.2690 nm, which corresponds to the interplanar spacing of $GdVO_4$ (112) planes, agreeing well with the d (112) spacing of the literature value (0.2694 nm; JCPDS no. 17-0260). The result further confirms the formation of crystalline $GdVO_4$ in nanofibers after thermal treatment, agreeing well with the XRD results.

3.2. Luminescence properties

3.2.1. Photoluminescence properties

Fig. 6 exhibits excitation and emission spectra of $GdVO_4$:Ln^{3+} (Ln = Eu, Dy, Sm) nanofibers, respectively. The excitation spectrum (Fig. 6a) of $GdVO_4$:5 mol% Eu^{3+} nanofibers was obtained by monitoring the emission of the Eu^{3+} transition at 620 nm, ranging from 200 to 450 nm with a maximum peak at 276 nm due to VO_4^{3-} absorption. The intense peak at 276 nm is ascribed to a charge transfer from the oxygen ligands to the central vanadium atom within the VO_4^{3-} group ions [57]. From the viewpoint of molecular orbital theory, it corresponds to transitions from the $^1A_2(^1T_1)$ ground state to $^1A_1(^1E)$ and $^1E(^1T_2)$ excited states VO_4^{3-} ions [58].

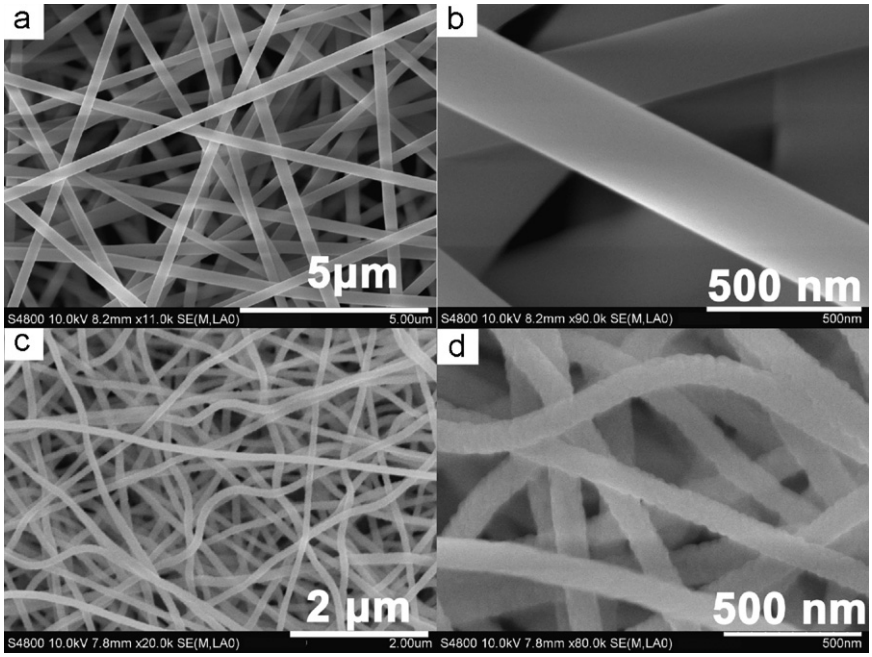

Fig. 4. SEM images of as prepared precursor fibers of $GdVO_4$:5 mol% Eu^{3+} (a) low magnification image and (b) high magnification image, and those annealed at 700 °C, (c) low magnification image and (d) high magnification image.

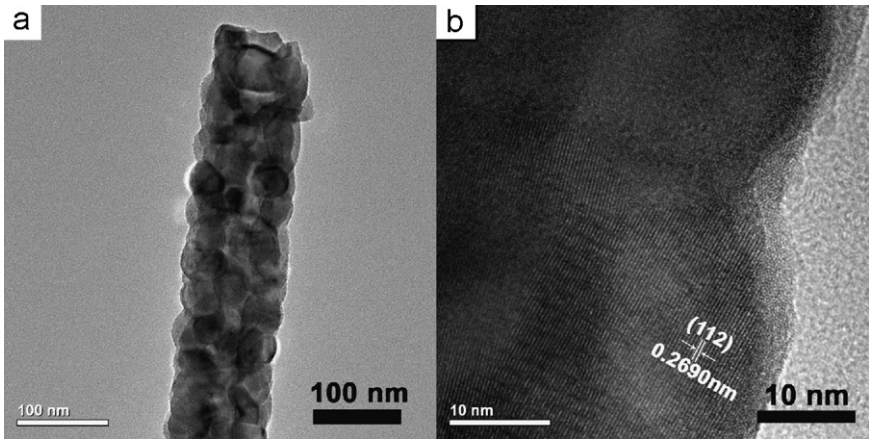

Fig. 5. TEM image (a) and HRTEM image (b) of $GdVO_4$:5 mol% Eu^{3+} nanofibers.

The presence of the strong VO_4^{3-} absorption band in the excitation spectra of Eu^{3+} indicates that there exists an efficient energy transfer from $GdVO_4$ host to the doped Eu^{3+} in $GdVO_4$:Eu^{3+} nanofibers. The emission spectrum (Fig. 6b) was obtained under short-wavelength UV irradiation when excitation into the VO_4^{3-} by a 276 nm irradiation. The emission spectrum shows typical emissions of Eu^{3+} ions in tetragonal $GdVO_4$, which corresponds to *f–f* transitions of Eu^{3+}. The most intense peak at 620 nm can be assigned to $^5D_0$–$^7F_2$ (red) transition. The emission spectrum not only contains the characteristic transition lines from the lowest excited $^5D_0$ level of Eu^{3+} but also those from higher energy levels ($^5D_1$, $^5D_2$, $^5D_3$) of Eu^{3+} with a very weak intensity. No emission from the VO_4^{3-} group is detected, suggesting that the energy transfer from VO_4^{3-} to Eu^{3+} is quite efficient. In addition, the crystal field splitting of Eu^{3+} $^5D_0$–$^7F_{1,2,4}$ transitions can be seen clearly, indicating that the $GdVO_4$:Eu^{3+} nanofibers are well-crystallized. Under UV excitation Dy^{3+} and Sm^{3+} doped $GdVO_4$ nanofibers exhibit yellow and orange-red emission, respectively. When monitored the emission of the Dy^{3+} at 620 nm ($^4F_{9/2}$–$^6H_{13/2}$) or Sm^{3+} at 604 nm ($^4G_{5/2}$–$^6H_{7/2}$), the excitation spectra (Fig. 6c and e) which have the similar profile as the excitation spectrum of $GdVO_4$:Eu^{3+} were obtained. A strong and broad band with a maximum at 276 nm come from VO_4^{3-} group also appeared. Excitation into the vanadate group at 276 nm yields the characteristic yellow emission (Fig. 6d) of Dy^{3+} at 484 nm ($^4F_{9/2}$–$^6H_{15/2}$, blue) and 574 nm ($^4F_{9/2}$–$^6H_{13/2}$, yellow) and orange-red emission (Fig. 6f) of Sm^{3+} at 567 nm ($^4G_{5/2}$–$^6H_{5/2}$, green), 604 nm ($^4G_{5/2}$–$^6H_{7/2}$, orange), and 649 nm ($^4G_{5/2}$–$^6H_{9/2}$, red), respectively. This indicates that, similar to the situations for Eu^{3+}, an efficient energy transfer also occurs from VO_4^{3-} to Dy^{3+} and Sm^{3+} in $GdVO_4$ nanofibers.

Fig. 7 displays the CIE chromaticity diagram of $GdVO_4$:Ln^{3+} (5 mol% Eu^{3+}, 2 mol% Dy^{3+}, 2 mol% Sm^{3+}). From the CIE chromaticity diagram, it can be seen that $GdVO_4$:5 mol% Eu^{3+} nanofibers emit in red region (CIE chromaticity coordinates $x=0.614$, $y=1.314$), $GdVO_4$:2 mol% Dy^{3+} nanofibers in yellow region (CIE chromaticity coordinates $x=0.379$, $y=0.416$), and $GdVO_4$:2 mol% Sm^{3+} nanofibers in orange-red region (CIE chromaticity coordinates $x=0.495$, $y=0.324$), respectively. The quantum efficiencies of $GdVO_4$:Ln^{3+} nanofibers are 14% (5 mol% Eu^{3+}), 6% (2 mol% Dy^{3+}), and 5% (2 mol% Sm^{3+}). In the preparation process of $GdVO_4$:Ln^{3+}

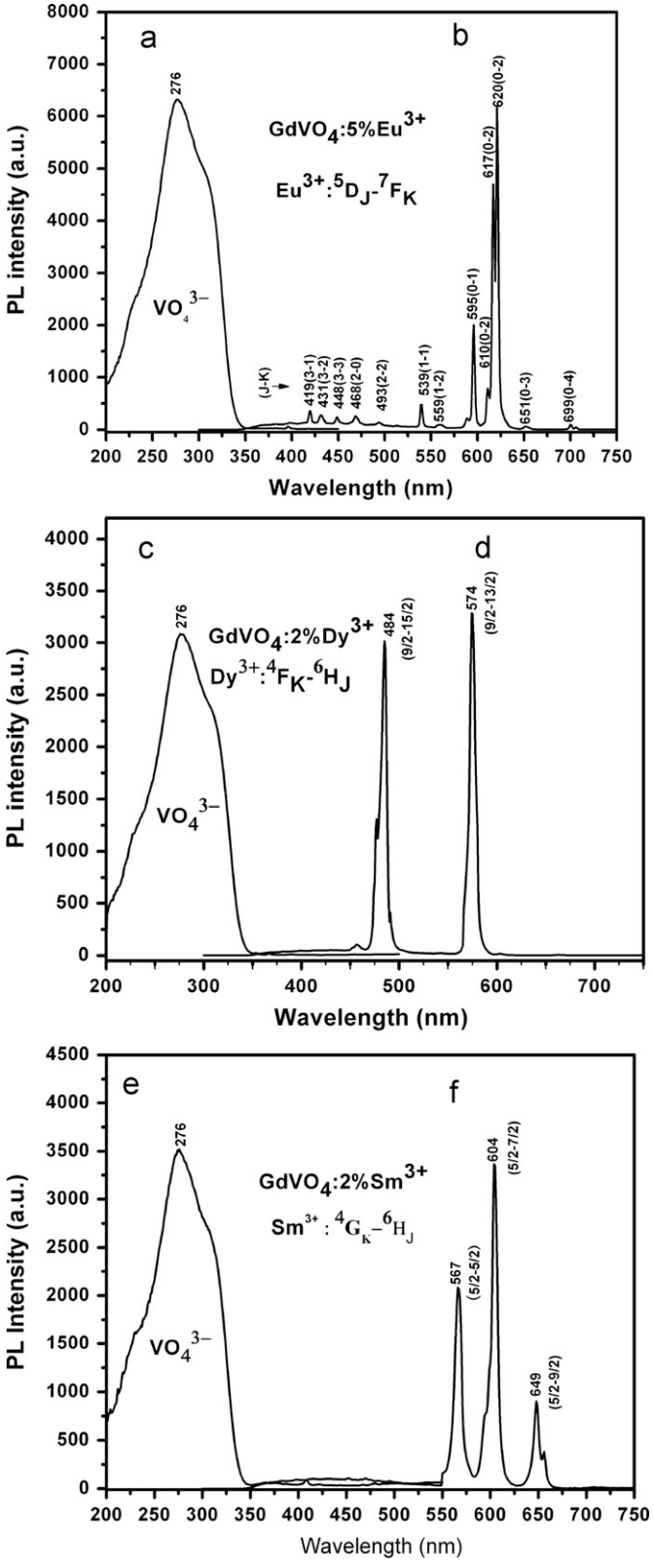

Fig. 6. PL (a, c, e) excitation and (b, d, f) emission spectra of $GdVO_4$ Ln^{3+} (Ln=5 mol% Eu, 2 mol% Dy, 2 mol% Sm) nanofibers annealed at 700 °C.

fiber–phosphors, large amount of organic species, such as PVP and citric acid were added in the precursor solution to adjust the viscosity in order to get the continuous fiber samples. After the final annealing process, most of the organic species can be removed accompanied by the crystallization of the samples. However, it is

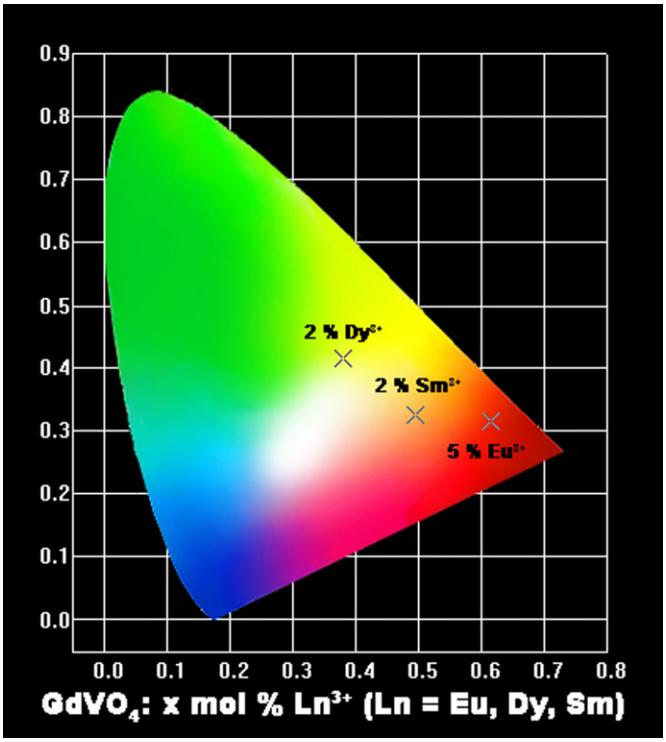

Fig. 7. The ClE chromaticity diagram of $GdVO_4$ Ln^{3+} (5 mol% Eu^{3+}, 2 mol% Dy^{3+}, 2 mol% Sm^{3+}) nanofibers annealed at 700 °C.

difficult to remove them completely, which is harmful for the luminescence of lanthanide ions (Ln^{3+}). This may lead to the low quantum efficiency (14%) in $GdVO_4$:Eu^{3+} fiber phosphors. For further improving the quantum efficiency of the sample, raising the annealing temperature may be an effective route, but too high annealing temperature may destroy the fiber morphology of the sample. As a result, we have to choose a moderate high annealing temperature to keep the perfect fiber morphology in spite of the low quantum efficiency.

Here it is expected that the luminescence properties (emission color and peak positions) of Ln^{3+} (Eu^{3+}, Dy^{3+}, Sm^{3+}) in 1D nanostructures of $GdVO_4$ will not be much different from other morphologies because the excitation and emission of Ln^{3+} arise from *f–f* transitions which are strongly shielded by the outside 5*s* and 5*p* electrons (but the emission intensity and quantum efficiencies may be of some differences). The reason for this effect is complicated and not very clear at this stage, which needs a large amount of detailed investigations in the future.

The photoluminescence decay curves for the representative emission of Eu^{3+} (620 nm, $^5D_0$–$^7F_2$) in $GdVO_4$:5 mol% Eu^{3+} nanofibers, Dy^{3+} (574 nm, $^4F_{9/2}$–$^6H_{13/2}$) in $GdVO_4$:2 mol% Dy^{3+} nanofibers, Sm^{3+} (604 nm, $^4G_{5/2}$–$^6H_{7/2}$) in $GdVO_4$:2 mol% Sm^{3+} nanofibers, are shown in Fig. 8. The decay curves for $^5D_0$–$^7F_2$ of Eu^{3+} (Fig. 8a), $^4F_{9/2}$–$^6H_{13/2}$ of Dy^{3+} (Fig. 8b), and $^4G_{5/2}$–$^6H_{7/2}$ of Sm^{3+} (Fig. 8c) can be well fitted into a double-exponential function as $I=A_1\exp(-t/\tau_1)+A_2\exp(-t/\tau_2)$. The average luminescence lifetimes for Eu^{3+} $^5D_0$ state, Dy^{3+} $^4F_{9/2}$ state, and Sm^{3+} $^4G_{5/2}$ state can be determined by the formula as $\tau=(A_1\tau_1^2+A_2\tau_2^2)/(A_1\tau_1+A_2\tau_2)$, and the average luminescence lifetimes for Eu^{3+}, Dy^{3+}, and Sm^{3+} are determined to be 0.552, 0.127, and 0.424 ms, respectively. The double-exponential decay behavior of the activator is frequently observed when the excitation energy is transferred from the donor [59,60].

The dependence of the PL emission intensity on its doping concentration (x) in $Gd_{(1-x)}VO_4$:xLn^{3+} (Ln=Eu, Dy, Sm) nanofibers was shown in Fig. 9a–c, respectively. By varying the content of the rare earth ions (Eu^{3+}, Dy^{3+}, and Sm^{3+}) in the $GdVO_4$ nanofibers, we

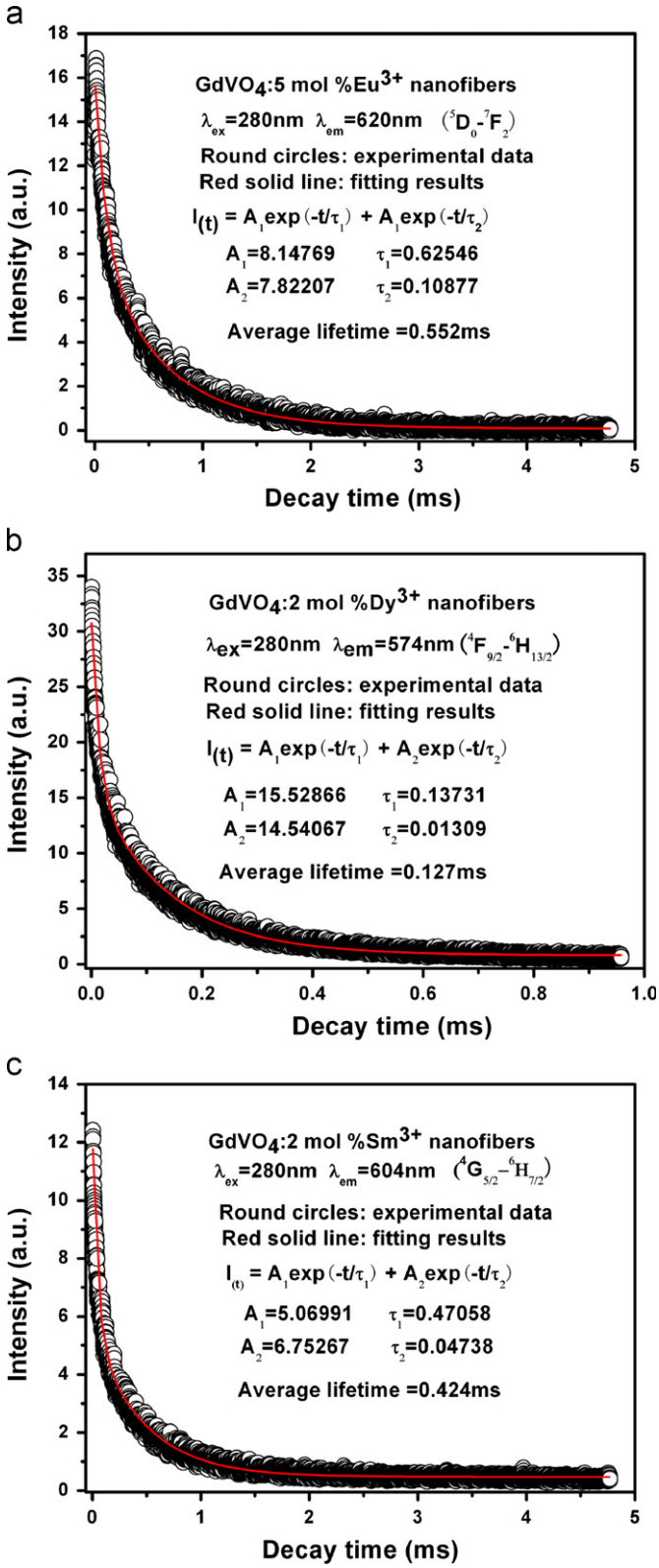

Fig. 8. Luminescence decay curves for Eu^{3+} (5 mol%, a), Dy^{3+} (2 mol%, b), and Sm^{3+} (2 mol%, c) in $GdVO_4$ nanofibers.

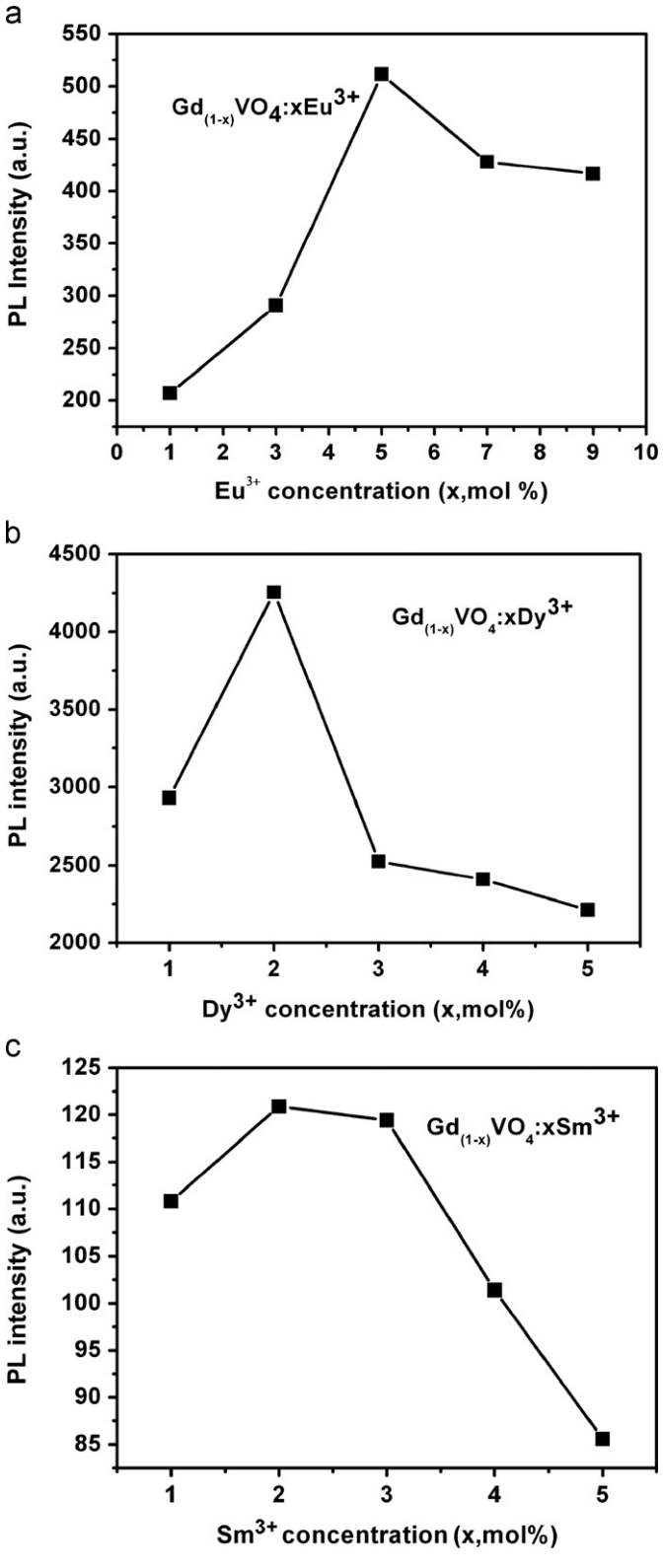

Fig. 9. PL emission intensity of Ln^{3+} as a function of its concentration (x) in $Gd_{(1-x)}VO_4{:}xLn^{3+}$ [Ln=Eu (a), Dy (b), Sm (c)] nanofibers annealed at 700 °C.

determined the compositions with the highest PL emission intensity. From Fig. 9, it can be found that the PL emission intensity of Eu^{3+} (Fig. 9a), Dy^{3+}(Fig. 9b), and Sm^{3+}(Fig. 9c) increase with the increase in their concentration (x) first, reaching a maximum value at x=5 mol% for Eu^{3+} and at x=2 mol% for Dy^{3+} and Sm^{3+}, respectively, and then decrease with the increase in their concentration (x) due to the concentration quenching effect. Thus, the optimum concentration for Eu^{3+} is 5 mol% and those for Dy^{3+}, Sm^{3+} are 2 mol% in $GdVO_4$ nanofibers phosphors, respectively. The low critical quenching concentration of Dy^{3+} and Sm^{3+}

may be caused by the cross-relaxation effect of these two ions, i.e., Dy^{3+} ($^4F_{9/2}$)+Dy^{3+} ($^6H_{15/2}$)→Dy^{3+} ($^6F_{3/2}$)+Dy^{3+} ($^6H_{9/2,\ 11/2}$), Sm^{3+} ($^4G_{5/2}$)+Sm^{3+} ($^6H_{5/2}$)→2Sm^{3+} ($^4F_{9/2}$). In general, the cross-relaxation effect will make the activator ion have a low quenching concentration [38]. No such cross-relaxation exists for Eu^{3+}, so it has a relatively high quenching concentration. The average distances (R) between Ln^{3+} ions can be estimated in terms of the equation $R=2(3V/4\pi XN)^{1/3}$ (where V is the volume of the unit cell, X is the concentration, and N is the number of available crystallographic sites occupied by the activator ions in the unit cell) [61]. The corresponding R (Ln^{3+}–Ln^{3+}) values for $Gd_{(1-x)}VO_4$:xLn^{3+} (x=5 mol% Eu^{3+}, 2 mol% Dy, 2 mol% Sm) nanofibers are calculated (the related crystal parameters V=0.330 nm^3, Z=4, and N=Z × 1=4). The average distances (R) between Eu^{3+} ions is 1.466 nm when the doping concentration reaches 5 mol% and those between Dy^{3+}, Sm^{3+} are 1.990 nm when doping concentration reaches 2 mol%, respectively.

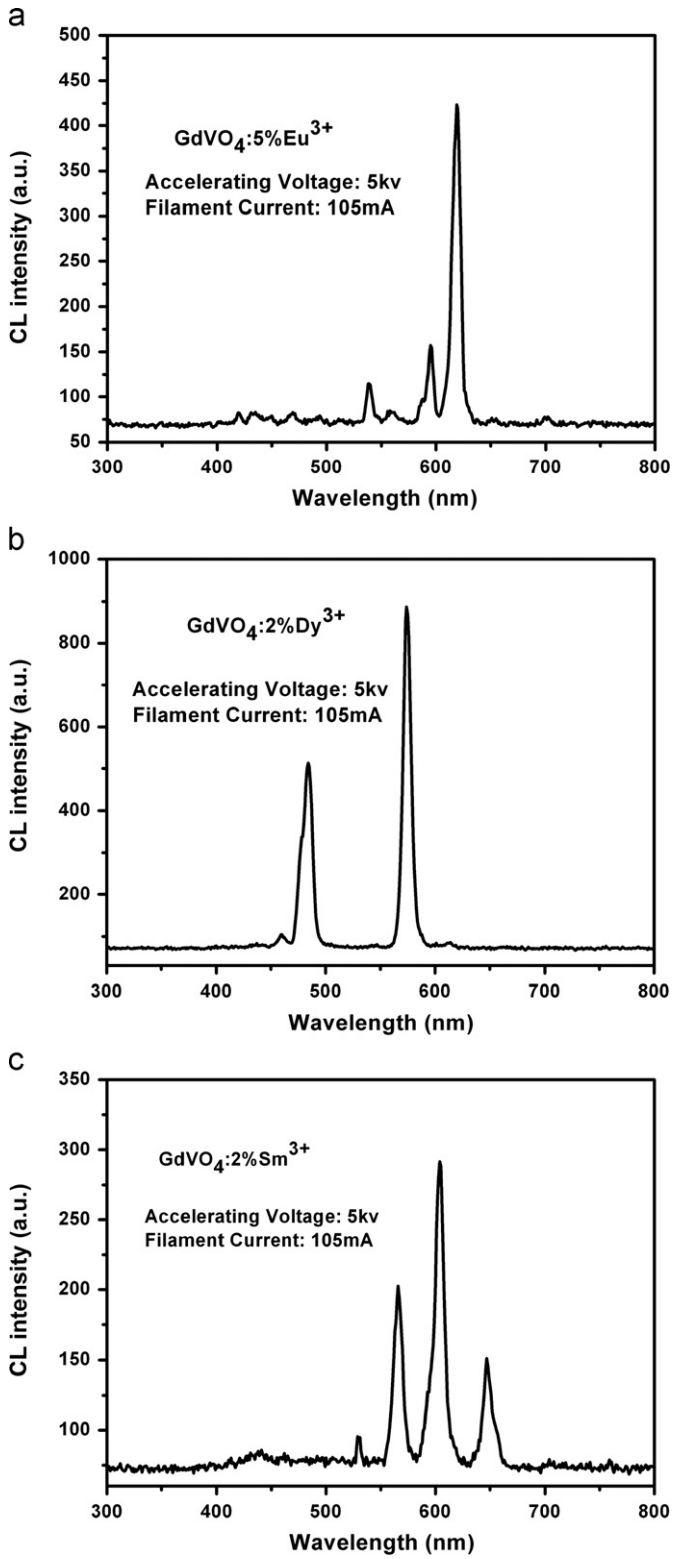

Fig. 10. Representive CL spectra of $GdVO_4$:5 mol% Eu^{3+} (a), $GdVO_4$:2 mol% Dy^{3+} (b), $GdVO_4$:2 mol% Sm^{3+} (c) nanofibers. (Accelerating voltage=5.0 kV, filament current=105 mA).

3.2.2. Cathodoluminescence properties

The CL spectrum properties of resulting samples were further investigated. The representive CL spectrum of $GdVO_4$:Ln^{3+} (Ln=Eu, Dy, Sm) nanofibers is shown in Fig. 10, which have identical shape as the PL emission spectrum. Thus, under the low-voltage electron beam excitation, the as prepared $GdVO_4$:5 mol% Eu^{3+} (Fig. 10a), $GdVO_4$:2 mol% Dy^{3+} (Fig. 10b), $GdVO_4$:2 mol% Sm^{3+} (Fig. 10c) nanofibers also show strong red, yellow, and orange-red emissions. The CL emission intensity for $GdVO_4$:Ln^{3+} (Ln=5 mol% Eu, 2 mol% Dy, 2 mol% Sm) nanofibers have been investigated as a function of the filament current and accelerating voltage, as shown in Fig. 11. When the filament current is fixed at 105 mA, the CL intensity

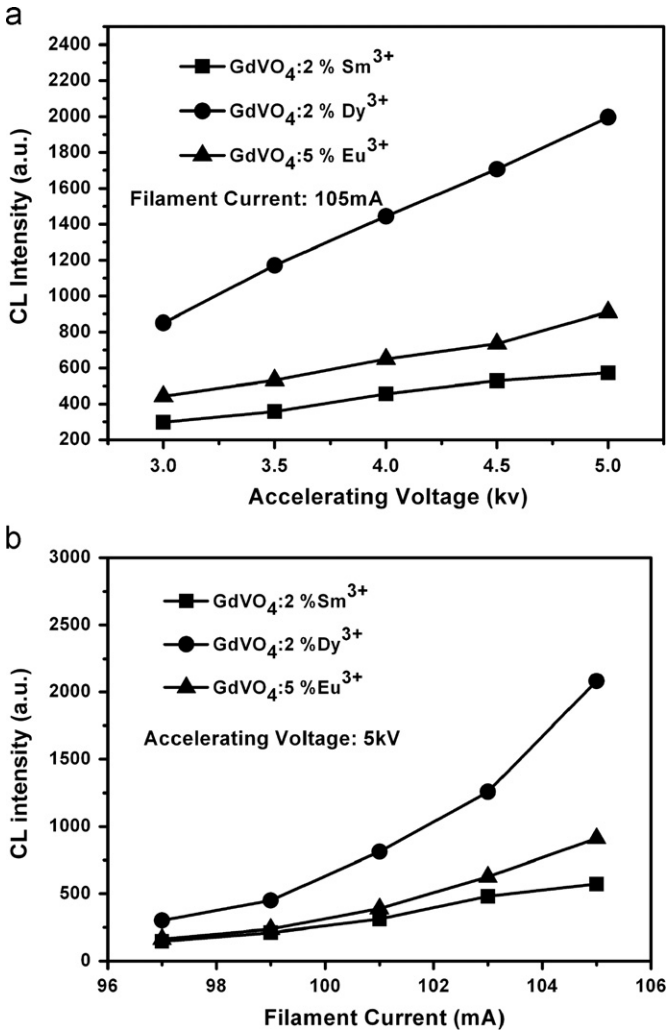

Fig. 11. The CL emission intensity for 5 mol% Eu^{3+}, 2 mol% Dy^{3+}, and 2 mol% Sm^{3+} doped $GdVO_4$ nanofibers as a function of the accelerating voltage (a) and filament current (b).

increases with increase in the accelerating voltage from 3.0 to 5.0 kV (Fig. 11a). Similarly, when the accelerating voltage is maintained at 5 kV, the CL intensity increases with raising the filament current from 97 to 105 mA (Fig. 11b). The increase in CL brightness with an increase in electron energy and filament current are attributed to the deeper penetration of the electrons into the phosphors and the larger electron beam current density. The electron penetration depth can be estimated using the empirical formula $L\,[\text{Å}]=250(A/\rho)(E/Z^{1/2})^n$, where $n=1.2/(1-0.29\log Z)$, A is the atomic or molecular weight of the material, ρ is the bulk density, Z is the atomic number or the number of electrons per molecule in the case compounds, and E is the accelerating voltage (kV) [62]. For cathodoluminescence, the Eu^{3+}, Dy^{3+}, and Sm^{3+} ions are excited by the plasmons produced by the incident electrons. The deeper the selectron penetration depth, the more plasmons will be produced, which results in more Eu^{3+}, Dy^{3+}, and Sm^{3+} ions being excited and thus the CL intensity increases.

4. Conclusions

In summary, one-dimensional $GdVO_4$:Ln^{3+} (Ln=Eu, Dy, Sm) nanofibers were successfully prepared by means of electrospinning technique in conjunction with sol–gel process. As prepared precursor samples present uniform fiberlike morphology and smooth surface with a length of several tens to hundreds of micrometers and diameters ranging from 230 to 460 nm. After precursor annealed at 700 °C for 4 h, the as-formed samples are well-crystallized with their fiberlike morphology. These as-formed $GdVO_4$:Ln^{3+} nanofibers consist of linked nanoparticles with the diameters ranging from 100 to 160 nm. The spectral and kinetic properties of those have also been investigated in detail. Under the short wavelength ultraviolet irradiation and the low-voltage electron beam excitation, $GdVO_4$:Ln^{3+} (Ln=Eu, Dy, Sm) nanofibers exhibit typical red, yellow, and orange-red emissions. The CL intensity increases with increase in accelerating voltage and filament current. The optimum doping concentration of Ln^{3+} (Ln=Eu, Dy, Sm) in the $GdVO_4$ nanofibers are 5, 2, and 2 mol%, respectively.

Acknowledgments

This project is financially supported by National Basic Research Program of China (Grant nos. 2007CB935502, 2010CB327704), and the National Natural Science Foundation of China (Grant nos. NSFC 50702057, 50872131, 20921002).

References

[1] M.H. Huang, S. Mao, H. Feick, H.Q. Yan, Y.Y. Wu, H. Kind, E. Weber, R. Russo, P.D. Yang, Science 292 (2001) 1897–1899.
[2] W.U. Huynh, J.J. Dittmer, A.P. Alivisatos, Science 295 (2002) 2425–2427.
[3] R. Ramaseshan, S. Sundarrajan, R. Jose, J. Appl. Phys. 102 (2007) 111101.
[4] Z.W. Pan, Z.R. Dai, Z.L. Wang, Science 291 (2001) 1947–1949.
[5] K. Tsukagoshi, B.W. Alphenaar, H. Ago, Nature 401 (1999) 572–574.
[6] D.F. Zhang, L.D. Sun, C.J. Jia, Z.G. Yan, L.P. You, C.H. Yan, J. Am. Chem. Soc. 127 (2005) 13492–13493.
[7] J. Hu, M.Y. Ouyang, C.M. Lieber, Nature 399 (1999) 48.
[8] D.S. Xu, G.L. Guo, L.L. Gui, Y.Q. Tang, E.J. Shi, E.X. Jin, Appl. Phys. Lett. 75 (1999) 481.
[9] J.R. Heath, P.J. Kuekes, n. Snyderg, Science 280 (1998) 717.
[10] H.W. Song, L.X. Yu, S.Z. Lu, Opt. Lett. 30 (2005) 483.
[11] H. Zhang, H.W. Song, H.Q. Yu, J. Phys. Chem. C 111 (2007) 6524.
[12] H. Zhang, H.W. Song, H.Q. Yu, Appl. Phys. Lett. 90 (2007) 103103.
[13] H.Q. Yu, H.W. Song, G.H. Pan, J. Lumin. 124 (2007) 39.
[14] M. Yazawa, M. Koguchi, A. Muto, M. Ozawa, K. Hiruma, Appl. Phys. Lett. 61 (1992) 2051.
[15] S.Y. Bae, H.W. Seo, J. Park, H. Yang, J.C. Park, S.Y. Lee, Appl. Phys. Lett. 81 (2002) 126.
[16] L. Fu, Y.Q. Liu, P. Hu, K. Xiao, G. Yu, D.B. Zhu, Chem. Mater. 15 (2003) 4287.
[17] J.G. Yu, J.C. Yu, W.K. Ho, L. Wu, X.C. Wang, J. Am. Chem. Soc. 126 (2004) 3422.
[18] T.J. Trentler, K.M. Hickman, S.C. Goel, A.M. Viano, P.C. Gibbons, W.E. Buhro, Science 270 (1995) 1791.
[19] J.H. Jung, H. Kobayashi, K.J.L. Van Bommel, S. Shinkai, T. Shimizu, Chem. Mater. 14 (2002) 1445.
[20] Y.C. Choi, W.S. Kim, Y.S. Park, S.M. Lee, D.J. Bae, Y.H. Lee, G.S. Park, W.B. Choi, N.S. Lee, J.M. Kim, Adv. Mater. 12 (2000) 746.
[21] X.F. Duan, C.M. Lieber, Adv. Mater. 12 (2000) 298.
[22] Z.G. Bai, D.P. Yu, H.Z. Zhang, Y. Ding, X.Z. Gai, Q.L. Hang, G.C. Xiong, S.Q. Feng, Chem. Phys. Lett. 303 (1999) 311.
[23] C.C. Chen, C.C. Yeh, Adv. Mater. 12 (2000) 738.
[24] Y. Wu, P. Yang, Chem. Mater. 12 (2000) 605.
[25] Y. Li, G.W. Meng, L.D. Zhang, F. Phillip, Appl. Phys. Lett. 76 (2000) 2011.
[26] J. Zhu, S. Fan, J. Mater. Res. 14 (1999) 1175.
[27] M.H. Huang, A. Choudrey, P. Yang, Chem. Commun. 12 (2000) 1603.
[28] A. Formhals, U.S. Patent 1975504.
[29] D. Li, Y. Xia, Nano Lett. 3 (2003) 555–560.
[30] B. Ding, H. Kim, C. Kim, M. Khil, S. Park, Nanotechnology 14 (2003) 532–537.
[31] D. Li, G. Ouyang, J.T. McCann, Y. Xia, Nano Lett. 5 (2005) 913–916.
[32] S. Madhugiri, A. Dalton, J. Gutierrez, J.P. Ferraris, K.J. Balkus, J. Am. Chem. Soc. 125 (2003) 14531–14538.
[33] P. Yang, C.F. Song, M.K. Lu, G.J. Zhou, Z.X. Yang, D. Xu, D.R. Yuan, J. Phys. Chem. Solids 63 (2002) 639–643.
[34] X.Y. Wang, C. Drew, S.H. Lee, K.J. Senecal, J. Kumar, L.A. Samuelson, Nano Lett. 2 (2002) 1273.
[35] H.Q. Liu, J. Kameoka, D.A. Czaplewski, H.G. Craighead, Nano Lett. 4 (2004) 671.
[36] D.A. Czaplewski, J. Kameoka, R. Mathers, G.W. Coates, H.G. Craighead, Appl. Phys. Lett. 83 (2003) 4836.
[37] C.L. Casper, J.S. Stephens, N.G. Tassi, D.B. Chase, J.F. Rabolt, Macromolecules 37 (2004) 573.
[38] G. Blasse, B.C. Grabmaier, Luminescent Materials, Springer-Verlag, Berlin, 1994.
[39] S. Shionoya, W.M. Yen, Phosphors Handbook, CRC Press, Boca Raton, 1999.
[40] D. Chen, Y.L. Yu, P. Huang, Z.F. Shan, L.W. Zeng, A.P. Yang, Y.S. Wang, Phys. Chem. Chem. Phys. 12 (2010) 7775–7778.
[41] Z.Y. Hou, P.P. Yang, C.X. Li, L.L. Wang, H.Z. Lian, Z.W. Quan, J. Lin, Chem. Mater. 20 (2008) 6686–6696.
[42] A.M. Pires, M.R. Davolos, E.B. Stucchi, Int. J. Inorg. Mater. 3 (2001) 785–790.
[43] A.I. Zaguniennyi, V.G. Ostoumov, I.A. Shcherbakov, T. Jensen, J.P. Meyn, G. Huber, J. Quant. Electron. 22 (1992) 1071–1072.
[44] P.J. Morris, W. Lulty, H.P. Weber, Y.D. Zavarstev, P.A. Studenikin, I. Shcherbakov, A.I. Zagumenyi, Opt. Commun. 111 (1994) 493.
[45] F. Wang, X.J. Xue, X.G. Liu, Angew. Chem. Int. Ed. 47 (2008) 906.
[46] J.H. Wu, B. Yan, J. Alloys Compd. 455 (2008) 485.
[47] R.C. Ropp, J. Electrochem. Soc. 115 (1968) 940.
[48] R.X. Yan, X.M. Sun, X. Wang, Q. Peng, Y.D. Li, Chem. Eur. J. 11 (2005) 2183.
[49] Y.P. Fang, A.W. Xu, R.Q. Song, H.X. Zhang, L.P. You, J.C. Yu, H.Q. Liu, J. Am. Chem. Soc. 125 (2003) 16025.
[50] X.F. Lu, Y.Y. Zhao, C. Wang, Adv. Mater. 17 (2005) 2485.
[51] J. Wu, J.L. Coffer, Chem. Mater. 19 (2007) 6266.
[52] Y.Y. Zhao, H.Y. Wang, X.F. Lu, X. Li, Y. Yang, C. Wang, Mater. Lett. 62 (2008) 143.
[53] N. Weinstock, H. Schulze, A. Muller, J. Chem. Phys. 59 (1973) 5063.
[54] A. Garcia-Murillo, C. Le Luyer, C. Dujardin, C. Pedrini, J. Mugnier, Opt. Mater. 16 (2001) 39–46.
[55] F. Zhou, X.M. Zhao, H. Xu, C.G. Yuan, J. Phys. Chem. C 111 (2007) 1651.
[56] K.X. Yao, H.C. Zeng, J. Phys. Chem. C 111 (2007) 13301.
[57] M. Yu, J. Lin, Z. Wang, J. Fu, S. Wang, H.J. Zhang, Y.C. Han, Chem. Mater. 14 (2002) 2224–2231.
[58] C. Hsu, R.C. Powell, J. Lumin. 10 (1975) 273–293.
[59] T. Fujii, K. Kodaira, O. Kawauchi, N. Tanaka, H. Yamashita, M. Anpo, J. Phys. Chem. B 101 (1997) 10631.
[60] W.Y. Shen, M.L. Pang, J. Lin, J.Y. Fang, J. Electrochem. Soc. 152 (2005) H25.
[61] G. Blasse, philips Res. Rep. 24 (1969) 131.
[62] C. Feldman, Phys. Rev. 117 (1960) 455.